



# Consolidated review of Structural and functional characterization of III-Sb quantum materials and devices

## Deliverable 4.7

**Version 1**  
**January 15<sup>th</sup> 2025**

**Authors:** QUANTIMONY is a collaborative training network and the scientific activities have been carried out thanks to the collaboration of many different individuals. The list below only reflects the contributors to the drafting of this deliverable.

Technical University Eindhoven (TUE): MSc Aurelia Trevisan (ESR7), Prof. Paul Koenraad (ESR7 main supervisor)  
University of Warwick (UOW): MSc. Francisco Alvarado César (ESR6), Prof. Richard Beanland (ESR6 main supervisor), Dr. Yisong Han (local co-supervisor)  
Agencia Estatal Consejo Superior de Investigaciones Científicas (CSIC): MSc. Giulio Barbieri (ESR1), MSc. Fernanda Malato (ESR2), Dr. Benito Alén (ESR1 main supervisor and network coordinator), Dr. Gema Martínez-Criado (ESR2 main supervisor), Dr. José M. Llorens (ESR1 local co-supervisor), Dr. Francisco J. Palomares (ESR2 local co-supervisor)

## Executive Summary

This deliverable is the final report of the scientific activities described in Table 3.1.a of our Work Plan for Work Package 4: Structural and Functional Analysis. Previous periodic progress reports were uploaded in M18 and M30 being this deliverable the consolidated review around the “Structural and functional characterization of III-Sb quantum materials and devices” for public dissemination.

The objective of WP4, led by Technical University of Eindhoven (TUE) is to unveil the physical properties of novel III-Sb quantum materials and devices using advanced characterization techniques.

ESR1 and ESR2 at CSIC, ESR6 at UOW and ESR7 at TUE contributed to this WP which had to further develop and apply the most precise structural and functional characterization techniques in different spatial, temporal and spectral domains.

## WP4.1: Atomic Level Characterisation of III-Sb Quantum Materials (Task Leader UOW)

### *ULTRARAM™ TBRT structures*

While ULTRARAM™ devices have demonstrated all these outstanding performance metrics [Hodgson2022], there are significant material challenges to overcome for the structure to be a manufacturable and viable device. An important contribution of Quantimony has been to assess UltraRAM material quality and develop protocols for quantitative compositional measurements at the atomic scale (Figure 1). The structure, as designed, is composed of binary compounds InAs and AlSb (Fig. W4.1.1a). The layers look flat and sharp in low magnification TEM images (Fig. W4.1.1c). However, even on these images the intensity profiles indicate a sluggish incorporation of Sb, with a distinctive curve at the lower interface of the AlSb collector (arrowed, Fig. W4.1.1b). Furthermore, when examined at the atomic scale (Fig. W4.1.1d) it becomes apparent that interfaces are not perfectly sharp, upper and lower interfaces are asymmetric (Fig. W4.1.1e) and that it is not even certain that the desired composition is attained, particularly for the central AlSb layer with a nominal thickness of only 1.2nm (i.e. 4 monolayers).

Characterisation of ULTRARAM™ structures and devices has been a collaborative effort between [ULANC \(ESR8\)](#), [UOW \(ESR6\)](#), [TUE \(ESR10\)](#) and partner organisation [Universidad de Cadiz \(UCA\)](#). There have been several secondments between these beneficiaries; [ESR8](#) was seconded to [UOW](#) [13-11-2023 to 13-12-2023], bringing several UltraRAM devices, working with [ESR6](#) to investigate structural aspects of device processing such as choice of dielectric and control of dry etch on device performance (Fig. W4.1.2). Although generating no publications, these interactions enabled improvements in device fabrication.

Atomic resolution characterisation of TBRT structures using aberration-corrected STEM has focused on obtaining a quantitative measure of composition that would allow the performance of real devices to be modelled. The gradual changes in composition at interfaces, and possibly the presence of ternary or quaternary compounds rather than the nominal binary compounds, may have a significant effect on the process window for viable devices. In the annular dark field (ADF)-STEM image of Figs. 1d and 1e each dot corresponds to a 'column' of atoms that runs through the thickness of the specimen. Group III and group V atoms appear in different columns in the [110] view shown in Fig. W4.1.1, and appear as a pair of dots known as a dumbbell. The intensity of these atom columns increases with mean atomic number; thus, in AlSb the Al atom columns have weak contrast while the Sb atom columns are bright, whereas in InAs the In atom columns are brighter than the As atom columns. However, the link between intensity and atomic number is not simple; the measured signal is due to electron-phonon scattering and the intensity of the propagating electron wave develops in a complex way as it propagates through the specimen. Thus, the actual contrast of an atom column depends not just on its mean composition, but the position of the different atoms along it, as well as the composition of adjacent atom columns.

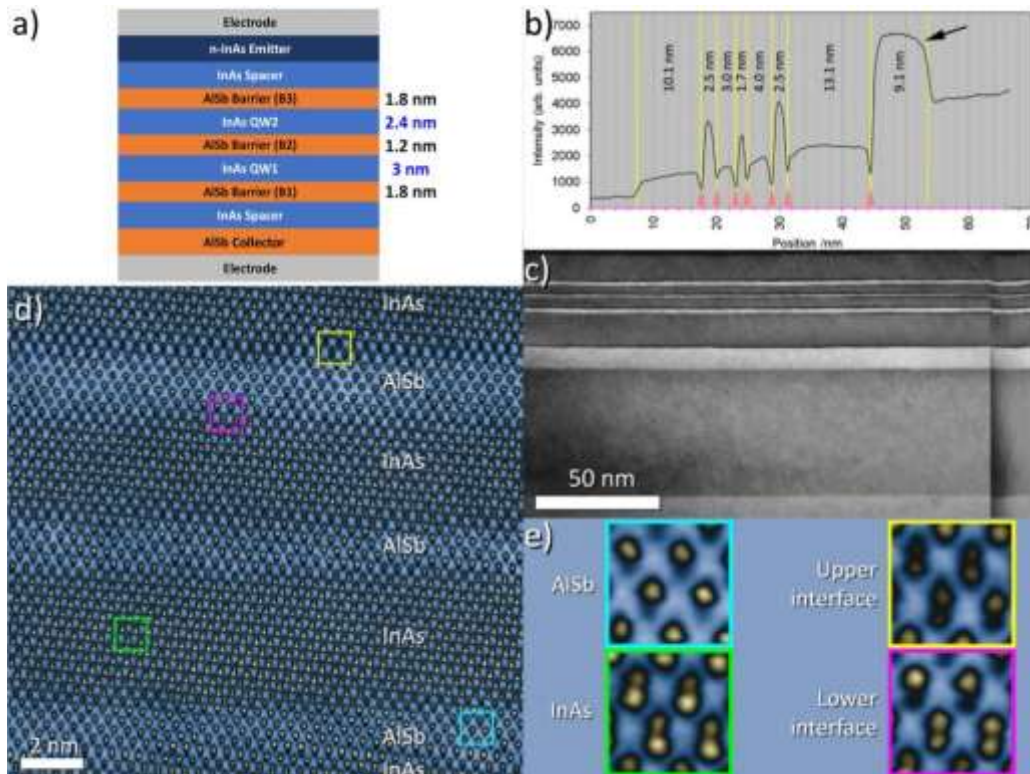


Figure W4.1.1. a) Nominal structure of an ULTRARAMTM InAs:AlSb:InAs:AlSb:InAs triple barrier resonant tunnelling (TRBT) structure. b) intensity profile across c), a dark field 002 image of a [110] cross section through an actual TRBT structure. d) false colour [110] atomic resolution ADF-STEM image of the TRBT structure. e) selected regions of d) showing the changes in atom column intensity corresponding to varying atomic number.

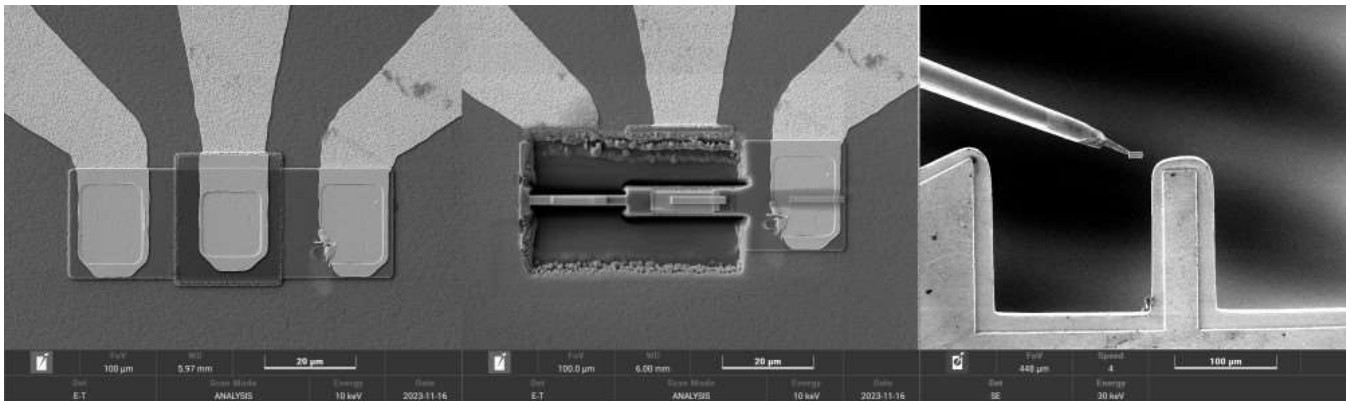


Figure W4.1.2. FIB preparation of an UltraRAM device for TEM investigation during the secondment of ESR8 to UOW. Left; the chosen device; centre, fabrication of lamellae; right, lamella lift out and attachment to a Cu support for TEM examination.

From this discussion it can be appreciated that the intensities of atom columns give an impression of the gradual changes in composition at interfaces, and varying compositions of the different layers in a TRBT structure, but a quantitative interpretation is not straightforward. To tackle this problem, ESR6 has investigated the ratio of the intensities of group III and group V atom columns  $F$  as a function of composition  $x$ ,  $y$  and specimen thickness  $t$ :

$$F(x, y, t) = \frac{I_{III} - I_V}{I_{III} + I_V}$$

Using multislice simulations and assuming a random alloy,  $F$  can be calculated for any composition and thickness. An example is given in Fig. W4.1.3b, showing the intensity ratio for  $Al_{1-x}Sb_x$  at a thickness of 23.7 nm, which corresponds to the experimentally determined specimen thickness using position-averaged

convergent beam electron diffraction (PACBED) patterns, shown in Fig. W4.1.3a. These diffraction patterns can be collected during collection of an ADF-STEM image using a camera that samples the part of the scattering pattern that passes through the central hole of the annular dark field detector, and have been shown to be a sensitive method to determine specimen thickness when compared with simulations.

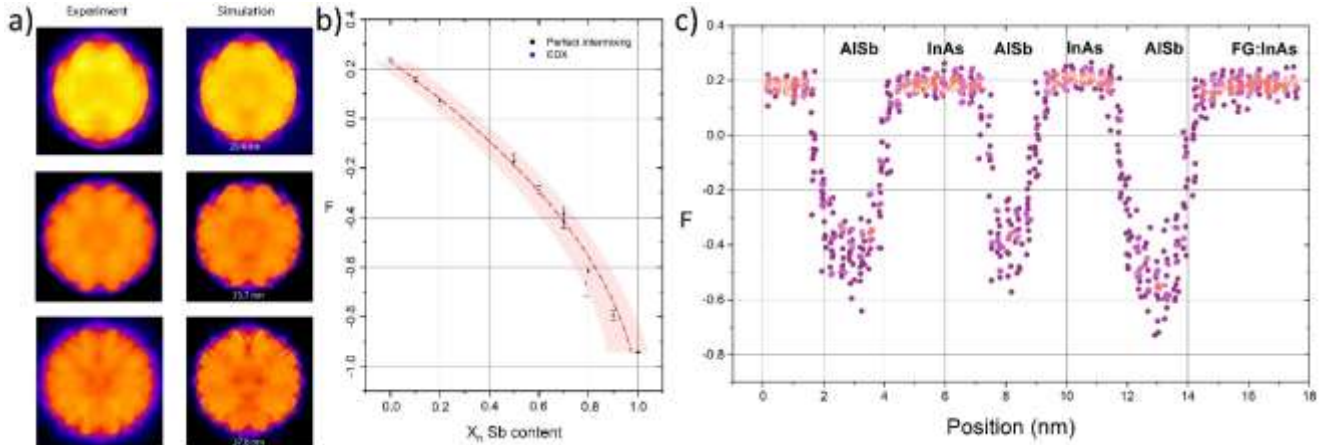


Figure W4.1.3. Quantification of composition in an ULTRARAM TBRT structure at UOW. a) PACBED measurement of specimen thickness. b) Multislice simulations of intensity ratio  $F$ . c) experimental measurement of  $F$  for an ULTRARAM structure. Top of the structure is to the right of the plot.

In Fig. W4.1.3b  $F$  is non-linear, with Sb atom columns having stronger contrast than would be expected if the intensity was proportional to atomic number alone. The red band indicates the range of intensities that were measured in the simulation, i.e. due to random variations in the composition of atom columns and the position of the different atom types within them. This variation is inescapable in a random alloy when measuring relatively small numbers of atoms and is also apparent in the experimental values of Fig. W4.1.3c. This shows a minimum  $F \approx -0.5$  in the first barrier,  $F \approx -0.4$  for the central barrier and  $F \approx -0.6$  for the upper barrier. Fig. W4.1.3b allows these values to be converted to  $\text{Al}_{0.3}\text{Sb}_{0.7}$ ,  $\text{Al}_{0.4}\text{Sb}_{0.6}$  and  $\text{Al}_{0.2}\text{Sb}_{0.8}$  respectively. These compositions are significantly different from the nominal binary value of AISb.

These measurements of composition taken from a single ADF-STEM image and are relatively quick and easy to perform. To qualify this method, compositions were also measured using Energy Dispersive X-ray spectroscopy (EDX), performed by ESR6 while on secondment to UCA [29-04-2023 to 03-06-2023] (Fig. W4.1.3d). This direct measurement of composition is a speciality of UCA and is far from straightforward, requiring perfect specimen preparation and long data acquisition times. The high energy density of the electron beam can produce radiation damage or changes in the specimen, and this was evident in these measurements, with loss of Al from the nominal AISb layers over many minutes of data acquisition. Nevertheless, by extrapolating the trends in apparent composition to zero time, a good measurement could be obtained (Fig. W4.1.4). These EDX compositions were in excellent agreement with the measurement made from the ADF-STEM image, which only required a few seconds of electron beam irradiation. This method therefore promises to allow estimates of composition at the atomic scale much more quickly and easily than EDX measurements, enabling rapid feedback to crystal growers who aim to reproduce the nominal design as an actualised device structure. Manuscripts are in preparation with ULANC, UOW and UCA co-authors.

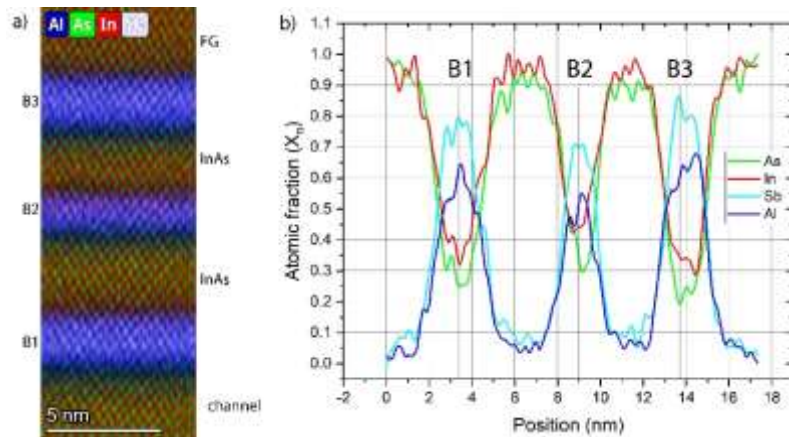


Figure W4.1.4. Quantification of composition in an ULTRARAM TBRT structure at UCA performed by ESR6 while on secondment. a) Atomic resolution EDX, b) line profile taken from (a) showing quantified compositions.

### Cross section scanning tunnelling microscopy of antimonides

Room temperature and low temperature cross section scanning tunnelling microscopy (X-STM) measurements were performed at TUE (ESR10) on an ULTRARAM™ sample provided by ULANC (ESR4). [Trevisan2023] The main goal of the experiment was to image the TBRT, giving another direct measurement of thickness, uniformity, interface sharpness and composition. X-STM is performed on a pristine surface under high vacuum, and an important restriction on the method is the need to produce such a surface inside the high vacuum chamber. Due to the irregular {111} cleavage of silicon, full ULTRARAM™ structures on silicon could not be examined; rather, equivalent structures on GaAs substrates were examined, which can cleave to produce large areas of atomically flat {110} facets. Figs. 5 and 6 shows the main result. A perfect surface could not be obtained and there is some loss of atoms from the surface (dark trenches). This is caused by the presence of defects (dislocations and stacking faults) that have formed due to unoptimized growth conditions, leading to internal misfit strains.

This version of the ULTRARAM structure has an  $\text{In}_x\text{Ga}_{1-x}\text{As}$  channel layer below the TBRT structure (dark blue in Fig. W4.1.5) that is under a small amount of tensile strain. The deleterious effect of this strain on growth morphology is apparent, with stacking faults and microtwins (only a few atomic layers in thickness) visible on {111} planes, often ending at the first AISb barrier but occasionally running across the whole TBRT. In the former case (Fig. W4.1.5, bottom), down-pointing triangle-shaped AISb regions were often associated with the microtwins, which indicate the disruption they introduced on the growth surface of the  $\text{In}_x\text{Ga}_{1-x}\text{As}$  layer. These “nanopits” only affect first AISb layer of the TBRT, which has a planar upper interface and thus an uneven thickness. Subsequent InAs and AISb layers in the TBRT are typically characterized by sharper interfaces and more uniform thickness.

Subsequently, also low temperature (LT) measurements on the same ULTRARAM™ TBRT sample were performed. All the different layers of the sample and most of the interfaces were measured, both at negative and positive bias. Most of the measured layers have good quality. Point defects were found only in the GaSb (hot) layer. In particular the point defects that have been observed are interstitial Sb atoms and iso-electronic As impurities. The interfaces that were possible to measure are sharp.

A height profile of the different layers gives some information on the strain in the structure (Fig. W4.1.6b). From the profile, it can be seen that the Sb containing layers relax outward while the  $\text{In}_x\text{Ga}_{1-x}\text{As}$  channel layer relaxes inward. If there was perfect pseudomorphic growth, the in-plane lattice constant of all layers above the GaAs would be fixed at the GaSb lattice constant. Therefore, the AISb barriers are compressively strained since AISb has a bigger lattice constant than GaSb (0.61355 and 0.60959 nm, respectively). Contrarily, InAs and  $\text{In}_{0.8}\text{Ga}_{0.2}\text{As}$  have smaller lattice constants (0.60583 and 0.59770 nm) than GaSb. The observed surface relaxation is consistent with these expectations, as shown by the calculated red line for these internal strains in Fig. W4.1.6b. While the X-STM measurements give dimensions and indications of strain, measurements of composition are not straightforward since sub-surface atoms contribute to the

tunnelling current. Nevertheless it is clear in Figs. 5 and 6 that there are non-uniformities in the TBRT layers with variations in contrast along the layer and individual Sb atoms, which appear bright due to their protrusion from the surface in Fig. W4.1.6, between the TBRT layers.

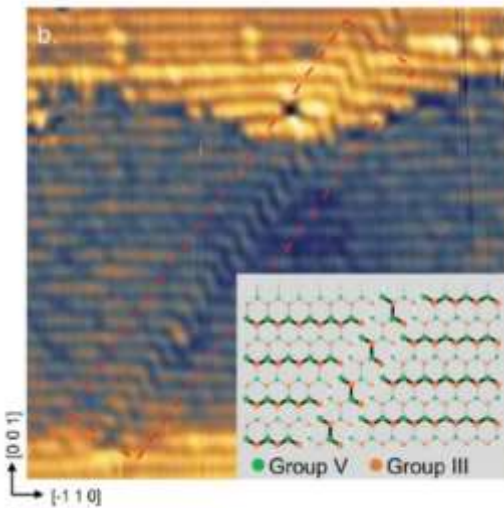
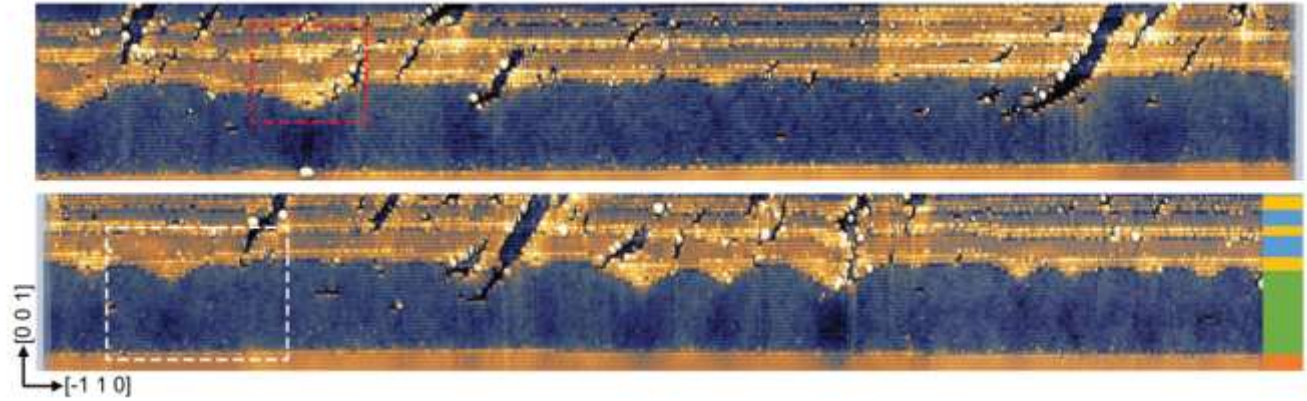


Figure W4.1.5. Top: 355–25 nm filled-state LT X-STM image of GaSb/InGaAs/TBRT, taken with a bias voltage  $V_b$  of 3 V and a tunnelling current  $I_t$  of 50 pA. The schematic structure of the layers is indicated on the right (colours match Fig. W4.1.1). The left image is the continuation of the top one. The darker areas that can be seen in the TBRT structure are ripped out part of the layers due to cleaving. Bottom: filled-state LT X-STM image showing a microtwin and its impact on the growth (structural model in inset).

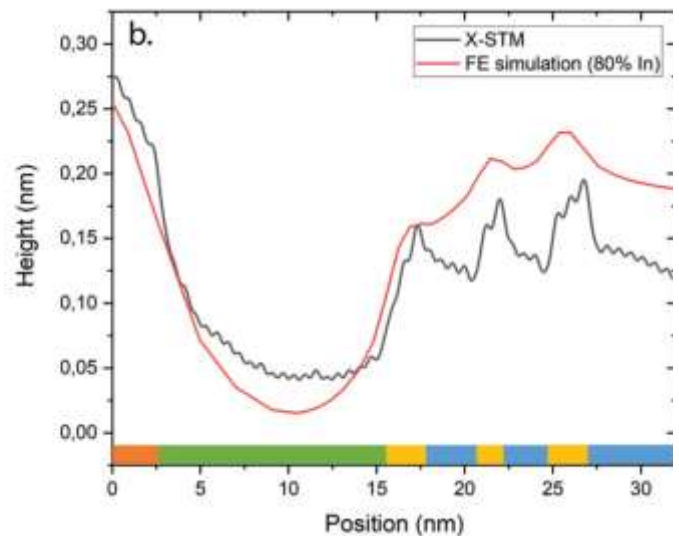
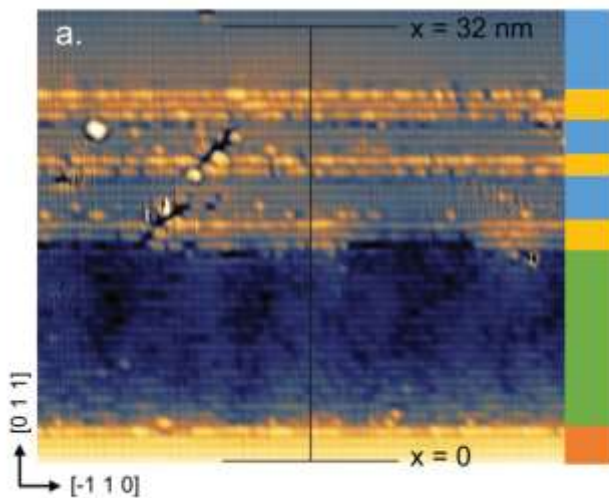


Figure W4.1.6. (a) 38–33 nm filled state LT X-STM image of an ULTRARAM TBRT,  $V_b = -3$  V,  $I_t = 50$  pA. The schematic structure of the layers is indicated on the right (colours match Fig. W4.1.1). (b) Height profile taken along the black line in (a) and the simulated profile for  $In_xGa_{1-x}As$  with  $x = 0.8$ .

X-STM measurements of antimonides have not been performed prior to this work and in order to quantify such data measurements have been performed at TUe (ESR7) on a GaAs/GaSb<sub>x</sub>As<sub>1-x</sub> multilayer sample provided by UPM (ESR3) (Figure 7). The growth of the sample was optimized to limit the Sb segregation. The goals of the experiment were to study the layers with low Sb content, investigating X-STM data from individual Sb atoms allowing their characteristics to be determined. The material was also examined by ESR7 with ESR6, using TEM during a secondment to UOW [5-11-2023 to 16-12-2023]. Fig. W4.1.7 shows a TEM image of the structure (top surface to the right) and Table I gives compositions obtained from high resolution X-Ray diffraction, fitting simulation to an experimental 004 rocking curve, and atom-counting X-STM measurements.



Figure W4.1.7. Bright-field  $g=004$  TEM image of the UPM multi-layer structure examined by ESR6 and ESR7 at UOW. The dark layers are GaAsSb while the lighter layers are GaAs. Dislocations at the interface of L1-L3 are highlighted by the dashed red oval.

Layer	XRD simulation [x%]	X-STM [x %]
L1	$0.2 \pm 0.2$	$0.14 \pm 0.02$
L2	$0.9 \pm 0.5$	$1.5 \pm 0.2$
L3	$2.0 \pm 0.5$	$2.3 \pm 0.3$
L4	$2.7 \pm 0.5$	
L5	$3.3 \pm 0.5$	
L6	$3.4 \pm 0.5$	
L7	$3.8 \pm 0.5$	

Table W.4.1. Compositions of GaSb<sub>x</sub>As<sub>1-x</sub> layers L1-L8

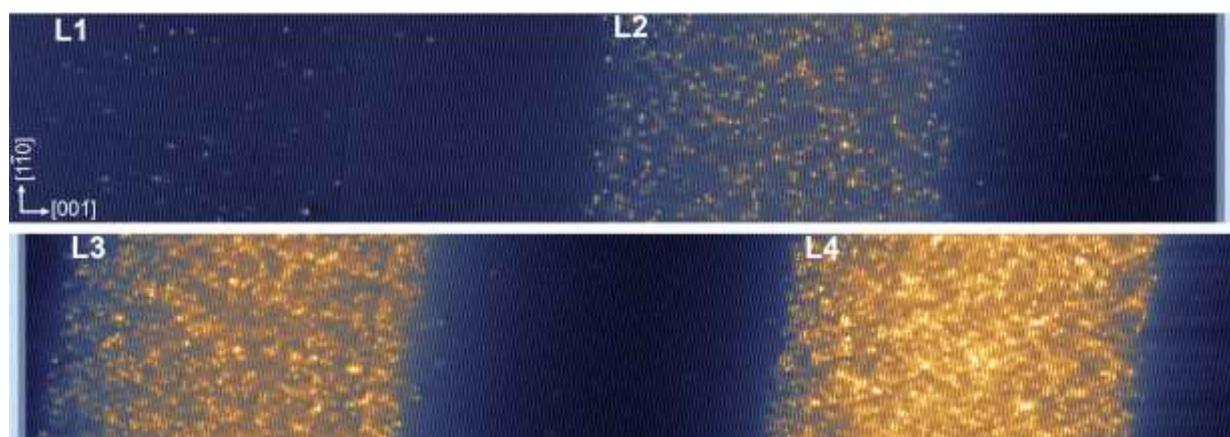


Figure W4.1.8.  $375 \times 32$  nm<sup>2</sup> filled-state LT X-STM image of L1, L2, L3 and L4,  $V_b = -3.00$  V,  $I_t = 50$  pA. The bottom part is the continuation of the top one.

As shown in Fig. W4.1.8, individual Sb atoms are readily resolved in layers L1 and L2, while for layer L4 with a composition of around  $x = 0.027$  the overlap between them is already sufficient to prevent quantitative analysis. However in L1 it was possible to identify six different type of contrast, labelled A to F in Fig. W4.1.9a. The symmetry and contrast of the features suggests the scheme shown in Fig. W4.1.9b. F has not

been classified but we believe that it might be an Ga vacancy. A manuscript is in preparation with UPM, UOW and TUE co-authors.

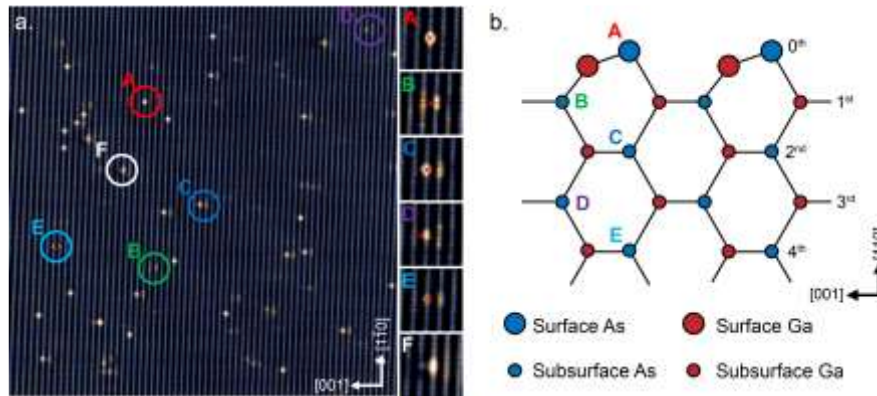


Figure W4.1.9.  $40 \times 40 \text{ nm}^2$  filled-state LT X-STM image from L1,  $V_b = -3.00 \text{ V}$ ,  $I_t = 50 \text{ pA}$ . Six different features (A to F) are highlighted by the circles

#### Cross section scanning transmission electron microscopy of quantum cascade lasers

Quantum cascade laser (QCL) structures grown by ESR10 at Julius-Maximilians-Universität Würzburg (UWUE) [Petrovic2024] have been analysed by ESR6 using TEM (Fig. W4.1.10). Like the ULTRARAM TBRT, these antimonide structures rely on very thin layers of different binary compounds for their functionality, which is usually modelled using perfectly sharp interfaces and binary compounds (e.g. NextNano simulation, Fig. W4.1.10 centre). However, these structures are also affected by segregation effects that are visible in atomic resolution ADF-STEM images (Fig. W4.1.10 right). Analysis of these data following a similar approach to that outlined for the TBRT structures is ongoing. A manuscript is in preparation with UWUE and UOW co-authors.

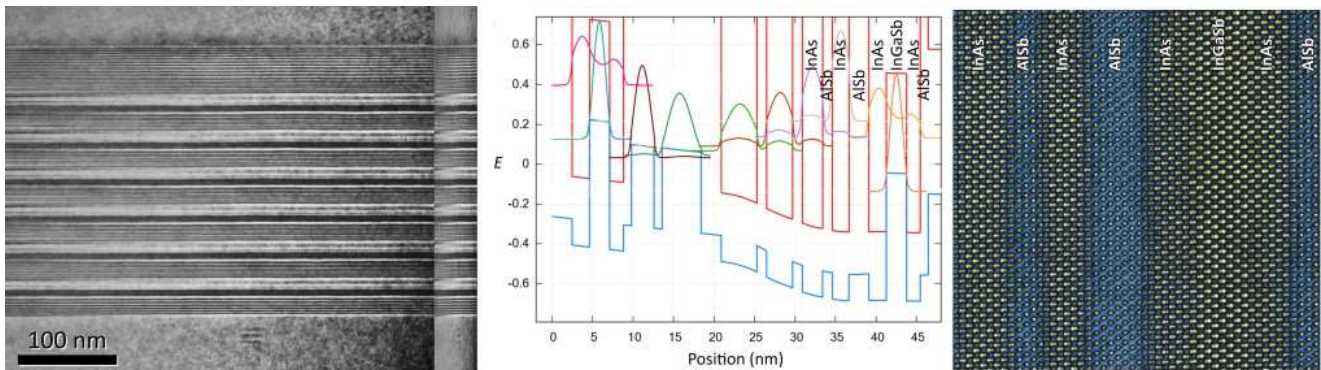


Figure W4.1.10. Left: Dark field  $g = 002$  TEM image of a six-period JMUW QCL structure. Centre: NextNano simulation of one QCL period. Right: false colour  $[110]$  atomic resolution ADF-STEM image of part of the structure.

#### Cross section scanning transmission electron microscopy of quantum ring vertical cavity surface-emitting diodes

Quantum ring (QR) structures have been grown by ESR6 at ULANC. These are future candidates for electrically driven ambient-temperature single-photon light-emitting diodes (SPLEDs) that can be mass-produced at low cost. Characterisation of these structures has been performed by ESR6 (UOW) using TEM (Fig. W4.1.11) and was taken by ESR6 to TUE for characterisation by X-STM, working with ESR7. The LED design employs a distributed Bragg transmitter (DBT) on the upper surface for enhanced light extraction, and simulations indicate close to 100% extraction of photons at the DBT resonance wavelength. Cross section TEM confirms the presence of GaSb quantum rings in the active region of the device (Fig. W4.1.11, right). However, examination of the material surface showed the presence of a significant density of defects (Fig. W4.1.11, left). Cross section TEM images showed that these were the result of microtwins that formed in the QR active region, disrupting subsequent growth in each layer of the DBT. Nevertheless, the majority of QRs are well-formed and defect free (Fig. W4.1.12) and the optical emission of the device with the DBT

structure is significantly stronger than an equivalent structure without (Fig. W4.1.12) [Acar2024]. A manuscript is in preparation with ULANC, UOW and TUE co-authors.

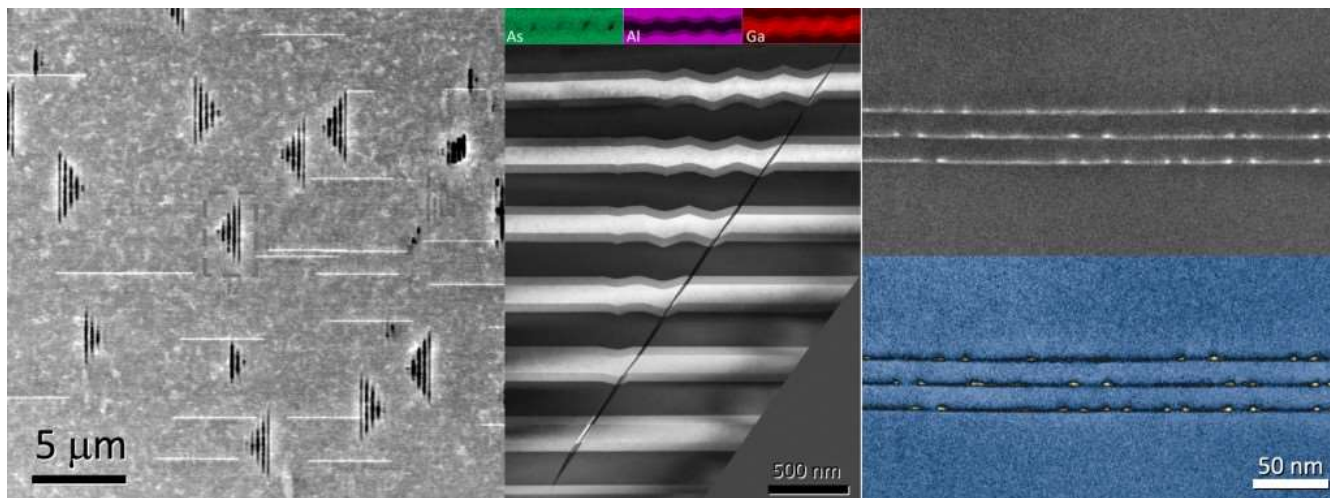


Figure W4.1.11. Left: Electron channelling contrast image of the surface of a QR-DBT structure showing a high density ( $\sim 3 \times 10^6 \text{ cm}^{-2}$ ) of 'arrow' defects and stacking faults (horizontal white lines). Centre: Dark field  $g = 002$  TEM image of the distributed Bragg transmitter showing wavy interfaces produced by a microtwin present in the material during growth. Right: dark field  $g = 002$  TEM image of the GaSb quantum rings in a GaAs matrix in the active region of the device. Lower image is shown in false colour to allow the QRs to be distinguished more readily.

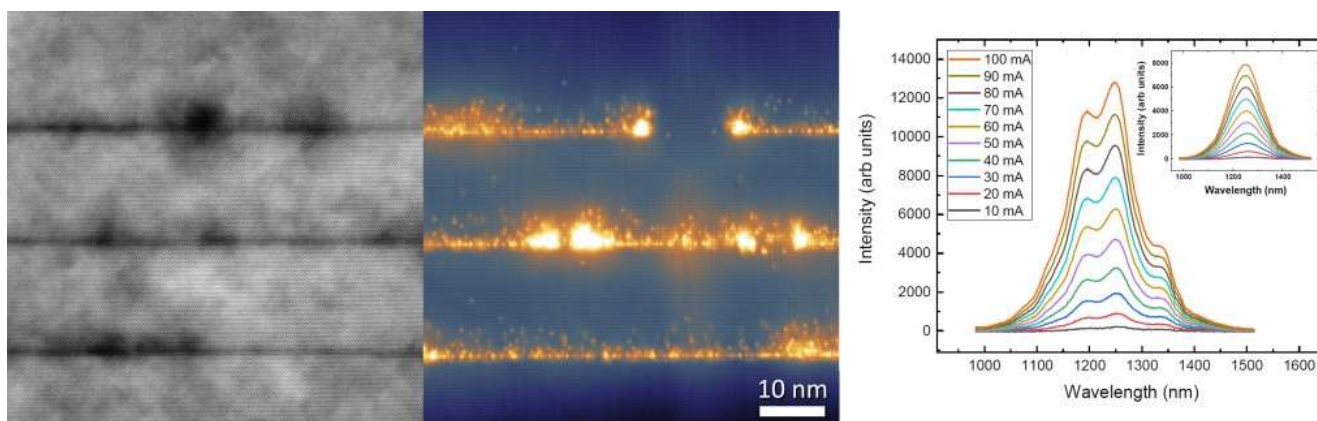


Figure W4.1.12. Left: High resolution TEM, centre: filled-state X-STM of GaSb QRs in GaAs matrix. Right: Electroluminescence intensity vs. wavelength for DBT QR LED (main) and normal QR LED (inset).

In summary, ESR6 and ESR7 projects focused on atomic level characterisation using scanning transmission electron microscopy and scanning tunnelling microscopy which has been applied to a variety of Quantimony materials, from ULANC, UPM, and UWUE. Secondments from ULANC and TUE to UOW, and UOW to TUE and UCA enabled cross-training in different methods and techniques, leading to collaborations between institutions on atomic level characterisation. This work has produced excellent results and the development of methodologies for atomic level characterisation including new ways of characterising composition from ADF-STEM images and classification of contrast from individual Sb atoms in X-STM.

## WP4.2: Nanoscale Characterization of III-Sb Quantum Materials and Devices (Task Leader: CSIC)

During this project, the research conducted by CSIC (ESR2) was organized into three main areas: (1) the characterization of InSb nanowire networks for quantum computing applications, (2) the exploration of InAs/GaAsSb quantum dots for high-efficiency photovoltaic technologies, and (3) an additional study focusing on

the origin of ultraviolet emission in  $\text{Zn}_2\text{GeO}_4/\text{SnO}_2$  nanowire heterostructures. To achieve these objectives, CSIC (ESR2) utilized the cutting-edge capabilities of the ID01 and ID16B beamlines at the partner organization ESRF (Grenoble). This methodology integrated the high spatial and spectral resolution provided by synchrotron nanobeams with a correlative analysis of multiple advanced X-ray techniques, including X-ray fluorescence (XRF), X-ray absorption near-edge spectroscopy (XANES), X-ray diffraction (XRD), and X-ray excited optical luminescence (XEOL). This comprehensive approach enabled a deeper understanding of the structural, chemical, and optical properties of the studied materials.

### InSb nanowire networks for quantum computing

InSb nanowire networks are highly promising candidates for integration into hybrid semiconductor-superconductor systems for quantum information processing devices, owing to their small effective mass, high Landé  $g$ -factor, and strong spin-orbit coupling. To date, the structural and compositional quality of these nanowire networks has been primarily studied using correlative high-resolution transmission electron microscopy and energy-dispersive X-ray spectroscopy on representative sample volumes. In this study, CSIC (ESR2) advanced the characterization of InSb multi-junction nanowire networks, grown using the in-plane selective area growth method (Prof. Erik Bakkers, TUe), through a comprehensive correlative analysis. This approach utilized spatially resolved scanning X-ray diffraction microscopy (SXDM), nano-XRF, and nano-XAS, enabling an in-depth evaluation of the crystal quality of the networks at the nanoscale.

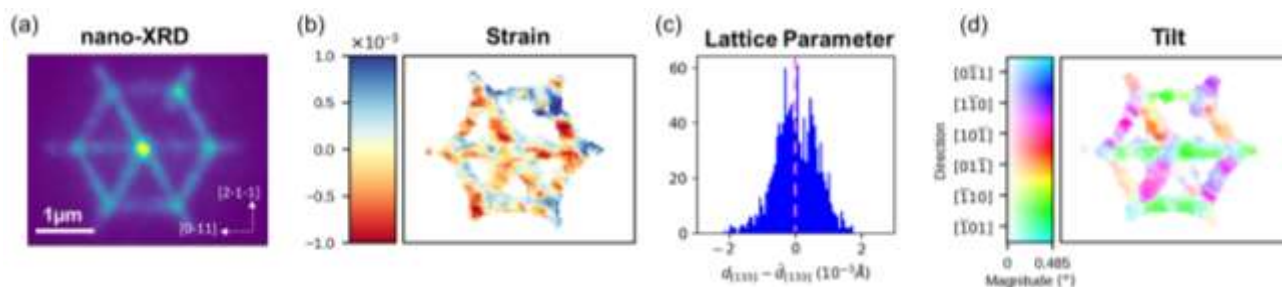


Figure WP4.2.1: Structural analysis. Maps of (a) the 133 Bragg peak intensity, (b) strain ( $\epsilon_{133}$ ), (c) lattice occurrence of displacements from the interplanar distance average, (d) lattice tilt distribution.

SXDM measurements (Figure WP4.2.1) revealed the presence of minor residual compressive strains within the nanowires. The spatially resolved analysis further uncovered deviations in crystal orientation at the junctions of the nanowires, highlighting the influence of the crossing points on the lattice structure in the InSb nanowire networks. Additionally, nano-XRF measurements demonstrated a homogeneous distribution of Sb across the nanowire network, with an enhanced Sb signal observed at the nanowire intersections (Figure WP4.2.2). This increase is attributed to material accumulation caused by overgrowth of InSb at the crossing points of the structure. To gain deeper insights into the local structure, nano-XANES was performed around the Sb K-edge. The spectra collected from various regions of the network exhibited shifts in the white line (primarily associated with  $1s \rightarrow 4p$  dipolar transitions), indicating changes in the Sb oxidation state. The data suggest an oxidation process occurring predominantly at the nanowire junctions, where the InSb overgrowth is most pronounced. These findings are of significant interest for understanding the transport properties of InSb nanowire networks and reinforce the potential of in-plane selective area growth as a viable method for producing high-quality InSb nanowire architectures. Such high structural integrity is essential for their prospective integration into quantum circuits.

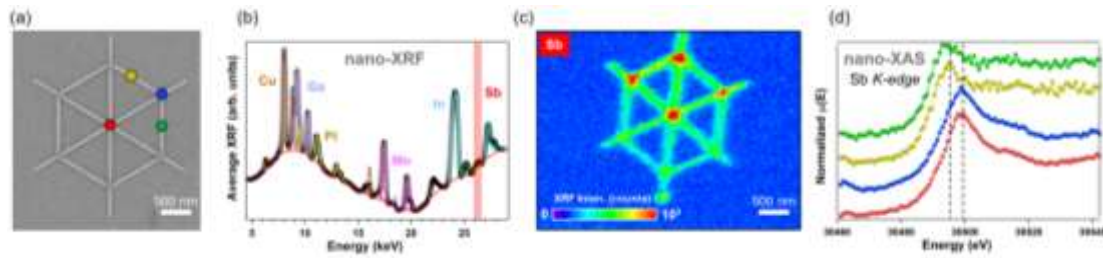


Figure WP4.2.2. Compositional and local structure analysis. (a) SEM image of a spider network. (b) Average X-ray fluorescence spectrum recorded over the spider network shown in (a) at 30.5 keV. (c) Individual Sb distribution map. (d) X-ray absorption near edge spectroscopy data recorded around the Sb K-edge. Each spectrum was collected on the point of the same colour marked on the network shown in (a).

### InAs/GaAsSb quantum dots for high-efficiency photovoltaic technologies

Covering InAs/GaAs quantum dots (QDs) with a thin GaAsSb strain-reducing capping layer (CL) enables fine-tuning of the QD morphology, band structure, carrier lifetime, and wavefunction topology, transitioning from a type-I to a type-II band alignment for Sb concentrations around 16%. These properties make GaAsSb CLs highly beneficial for enhancing the performance of optoelectronic devices based on InAs/GaAs QDs. However, conventional techniques such as transmission electron microscopy and related spectroscopies are typically limited to analyzing a cross-sectional area of only a few QDs. To date, spatially resolved in-plane material characterization of buried QDs within an actual device structure remains unexplored.

In this study, InAs/GaAsSb QD samples from UPM (ESR3) were analyzed using the ID16B beamline (Figure WP4.2.3). Nano-XRF revealed distinct regions with varying In intensity, suggesting an accumulation of QDs in areas with higher In signals. Meanwhile, the Sb distribution within the GaAsSb layers was remarkably homogeneous. Regarding the local environment of Sb, nano-XANES showed no significant changes in coordination or electronic states caused by QD formation. Comparisons between GaSb reference materials and GaAsSb layers revealed similar coordination environments, with a slight energy shift in the GaAsSb layers. This shift likely reflects shorter scattering-absorption distances due to the smaller bond lengths in the GaAs crystal structure. These findings provide valuable insights into the structural and compositional properties of GaAsSb capping layers and their influence on InAs QDs, critical for optimizing device performance.

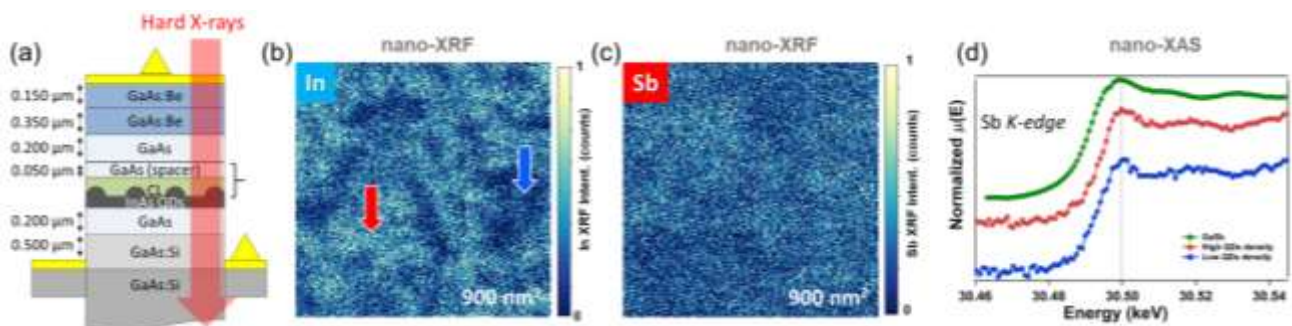


Figure WP4.2.3: InAs/GaAsSb quantum dot samples. (a) Device structure. Elemental maps that depicts the X-ray fluorescence intensities of (b) In and (c) Sb. (d) XANES data around the Sb K-edge taken in regions with low and high quantum dots density (marked with a blue and red arrow in (b) respectively).

### Ultraviolet emission in Zn<sub>2</sub>GeO<sub>4</sub>/SnO<sub>2</sub> nanowire heterostructures

Decorated semiconductor nanowires are highly promising architectures for next-generation nanoelectronic devices. Their versatile electronic, optical, and plasmonic properties make them ideal candidates for diverse applications, including quantum technologies, sensing, and energy harvesting. Among the various synthesis methods, the Plateau–Rayleigh (PR) crystal growth mechanism stands out, enabling the formation of intricate

decorated semiconductor nanowire systems. By precisely controlling the growth kinetics and deposition conditions, it is now possible to produce complex nanoscale systems with unconventional morphological characteristics, including periodicity, size modulation, and cross-sectional anisotropy. Since the performance of such heterostructures is closely tied to their crystal quality, it is essential to investigate their nanoscale physical properties, which can be significantly influenced by native defects, heterogeneities, and structural imperfections.

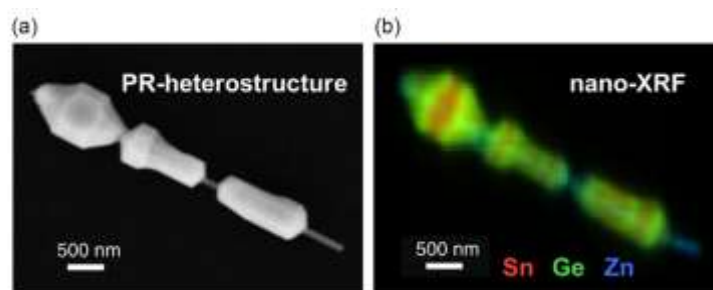


Figure WP4.2.4 Elemental distribution obtained by nano X-ray fluorescence (nano-XRF). (a) Scanning electron microscope (SEM) image of Plateau–Rayleigh (PR) heterostructure. (b) XRF map in RGB (Red, Green, Blue) visualization that depicts the XRF intensities of Sn (red), Ge (green), and Zn (blue). Their color brightness (light represents high counts, dark low counts) indicates the intensity ranges.

In this study, CSIC (ESR2) collaborated on an experiment to investigate the origin of ultraviolet (UV) emission in  $\text{Zn}_2\text{GeO}_4/\text{SnO}_2$  hybrid semiconductor nanowire heterostructures formed through the PR mechanism [Dolado2023a]. A combination of synchrotron nano-analysis techniques—nano-XRF, nano-XEOL, nano-XRD, and nano-XAS (Figures WP4.2.4 and WP4.2.5)—was employed to comprehensively study these structures.

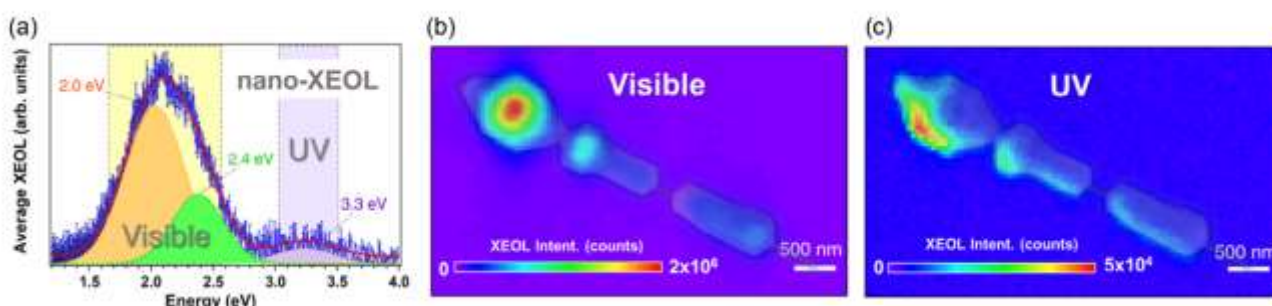


Figure WP4.2.5 X-ray-excited optical luminescence (XEOL) distribution with nanometric resolution. (a) Average XEOL spectrum recorded over the PR heterostructure shown in Figure WP4.2.4a. (b,c) XEOL-integrated intensity maps over the energy ranges defined by the colored bands (visible and UV) in (a).

The results revealed that the UV optical emission is likely driven by a Zn impurity-assisted process, which also involves the formation of a secondary phase within the  $\text{Sn}_{1-x}\text{Ge}_x\text{O}_2$  crystallites (Figure WP4.2.6). This study demonstrates that multimodal synchrotron nanoprobe techniques serve as an effective "all-in-one" approach for achieving an in-depth understanding of complex hybrid nanosystems, unraveling their atomic-scale and electronic properties with unparalleled precision.

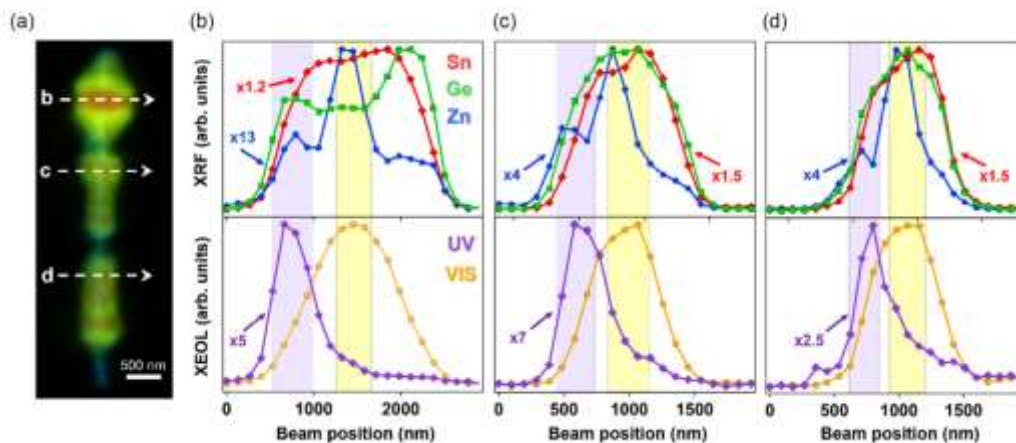


Figure WP4.2.6 Direct link between luminescence emissions and elemental distribution. (a) XRF nanoimage of PR heterostructure on which the line profiles were collected. (b–d) Normalized XRF line profiles (top) for Sn (red symbols), Ge (green symbols), and Zn (blue symbols), and XEOL line profiles (bottom) for visible (orange symbols) and UV (purple symbols) emissions. All profiles were collected along the white-dashed lines drawn on the PR heterostructure shown on the left-hand side, perpendicular to the central nanowire.

ESR2 also carried out in house XPS experiments with laboratory x-ray sources at ICM-SCIC to study the formation of silicide dots by ion beam irradiation of silicon surfaces with simultaneous metal supply. Depending on irradiation conditions (noble ion energy, fluence, incidence angle,...) a variety of self-assembled patterns developed which are deeply related to the surface stoichiometry. In addition, a collaborative project with the consortium beneficiary UWUE was started to study pyramidal surface defects in AlGaAsSb cladding layers in Interband Cascade Lasers, fabricated by ESR10 from UWUE. The experiment aimed to investigate the surface composition to correlate possible chemical inhomogeneities with the formation of the pyramidal defects. Complementary characterization by both Scanning electron microscopy and Auger Spectroscopy with lateral resolution (SAM) was also performed.

In summary, this project, carried out by CSIC (ESR2) in collaboration with ESRF, has deepened the understanding of complex Sb-based nanostructures for next-generation quantum, optoelectronic, and nanoelectronic devices. Utilizing advanced synchrotron-based techniques, CSIC (ESR2) successfully characterized intricate InSb nanowire and InAs/GaAsSb quantum dot systems, focusing on the critical role of Sb in growth mechanisms, compositional distribution, and local electronic environments. Furthermore, CSIC (ESR2) contributed to a study on  $Zn_2GeO_4/SnO_2$  nanowire heterostructures, further enhancing their expertise in synchrotron methodologies and broadening their analytical and fundamental knowledge of nanoscale material systems.

### WP4.3: Confocal Microspectroscopy of III-Sb Quantum Materials and Devices (Task Leader: CSIC)

During the project, ESR1 (CSIC) extensively used the equipment at IMN-CSIC's optics lab, gaining proficiency in advanced photoluminescence (PL) techniques. Following the installation of two superconducting nanowire single-photon detectors (SNSPD) and a new confocal head optimized for 900–1500 nm, ESR1 conducted 4 K ensemble photoluminescence (PL), micro-PL ( $\mu$ PL), time-resolved PL (TRPL), and polarization-resolved magneto-PL (MPL) on various epitaxially grown nanostructures. He also extensively performed 8-band k-p simulations, exploiting the in-house ZBKANE code and the commercial nextnano++. The former relies in an axially symmetric approximation resulting in a quasi-analytical model of fast execution, while the latter implements the full k-p method relying only on space discretization. The one-month secondment at nextnano GmbH strengthened the collaboration between the research group and the core developers of nextnano++, enabling us to obtain accurate numerical results across the project. Additionally, new ESR2 (CSIC), Simone Privitera, joined IMN-CSIC for seven months, where ESR1 introduced him to MPL techniques targeting spin-injection solutions in III-Sb devices, including superlattices

supplied by [Universidad Politécnica de Madrid \(UPM\)](#), setting the stage for further experiments in upcoming projects. [ESR5 \(ULANC\)](#), [Gizem Acar](#), also completed a one-month secondment at IMN-CSIC, conducting TRPL and ellipsometry experiments with [ESR1](#) on III-Sb quantum rings for single-photon emission.

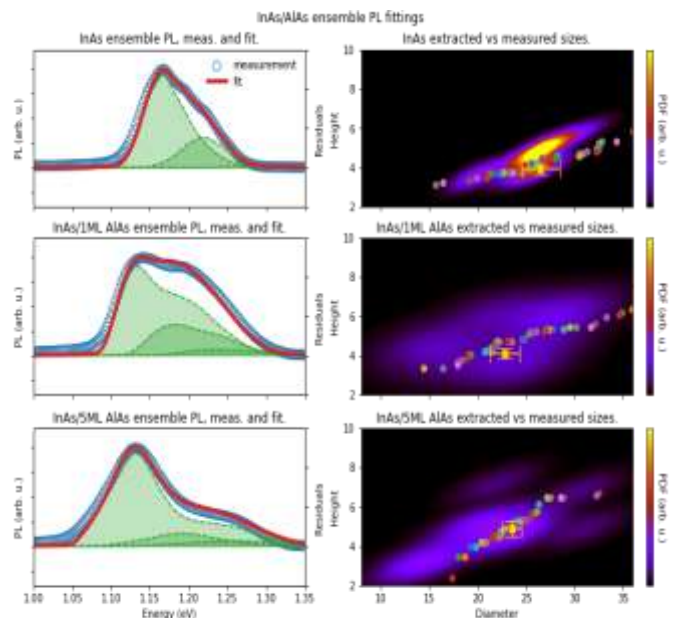
The integration of antimony (Sb) in III-V nanostructures opens exciting possibilities for advancing quantum technologies. By combining Sb's ability to red-shift emission into telecom bands with its large spin-orbit coupling (SOC) and hence, g-factor, these materials offer a promising platform for spin-photon interfaces and quantum light sources. The work carried out in this project focuses on leveraging these unique properties to address key challenges in the design, characterization, and optimization of III-Sb quantum dots (QDs) and related structures, providing a pathway toward the next generation of quantum devices.

### Capping Techniques for Tailoring Quantum Dot Optical Properties

SAQDs are promising candidates for solid-state quantum light sources. After its nucleation, the nanostructure can be capped with GaAs or with a different alloy, thus, allowing for engineering the QD properties. Capping the nanostructure with GaAsSb containing more than 20% Sb shifts the band alignment from type I to type II, resulting in a redshifted emission and an extended radiative lifetime. This method was investigated, in combination with electric fields, for manipulating hole wavefunction topology and optimizing g-factor tuning [Llorens2019].

SAQDs are promising candidates for solid-state quantum light sources. After its nucleation, the nanostructure can be capped with GaAs or with a different alloy, thus, allowing for engineering the QD properties. Capping the nanostructure with GaAsSb containing more than 20% Sb shifts the band alignment from type I to type II, resulting in a redshifted emission and an extended radiative lifetime. This method was investigated, in combination with electric fields, for manipulating hole wavefunction topology and optimizing g-factor tuning [Llorens2019]. A limitation of this proposal is the carrier escape due when large electric fields are applied. A possible solution is to introduce AIAs layers, which not only increase the potential height but also reduce the thermal coupling between QDs and the wetting layer (WL) formed during growth. Therefore, we started a study on InAs QDs with varying AIAs-capping thicknesses. Samples were grown by [UPM](#) and analyzed via HRTEM by QUANTIMONY partner [Universidad de Cádiz \(UCA\)](#). Ensemble PL spectra from these samples were broad and featureless, limiting the ability to correlate optical data with electronic and magneto-optical properties strongly influenced by their size, shape, and composition. To address this, [ESR1](#) developed the PhotoLuminescence to Structural Parameters (PL2SP) tool, so to extract QD size, shape, and composition distributions from ensemble PL data quickly and non-destructively, providing real-time feedback on fabrication across different growth runs.

PL2SP exploits low- and high-power ensemble PL measurements as input, combining them with 8-band k-p simulations from ZBKANE. 3D simulations within a predefined solution space yield the main transition energies and oscillator strengths, which form a fine-mesh grid of the electron-hole-pair (eh-pair) shell structure. By convoluting these states with a probability distribution of QD parameters and scaling excited-state contributions, the tool generates synthetic PL spectra for comparison. Using multi-objective genetic-algorithm minimization, PL2SP determines the parameter distribution that best fits experimental data. In Fig. W4.3.1 we show the high-power experimental PL of



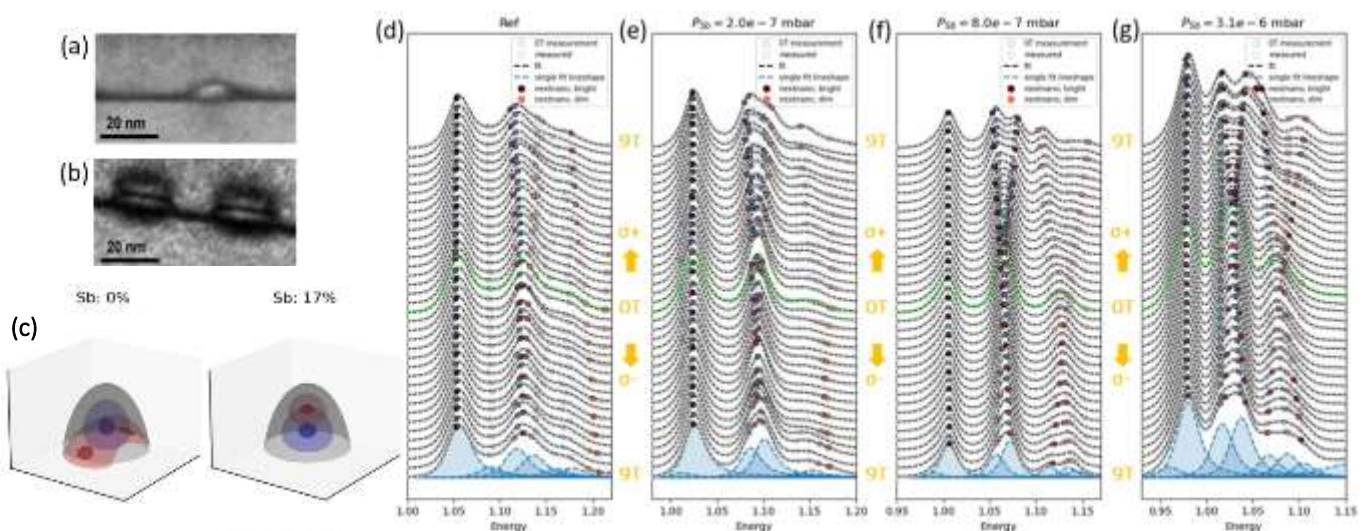
W4.3.1 Left column: high-power PL spectra (blue circles) with fit (red) of InAs/GaAs with varying AIAs capping thickness (rows). The fit given by the sum of the broadened groundstate and the relative excited states, opportunely scaled, each shown as the shaded green area. Right column: parameter probability distribution (shaded area) generating generating the fit on the left column. Experimental TEM values are shown as overlaid spots.

the AIAs-capped QDs compared to the generated spectra, together with the related parameter distribution, which aligned well with HRTEM measurements. PL2SP was also applied to type I and type II GaAsSb-capped QDs, and compared to TEM measurements [Barbieri2022]. Both studies are part of a manuscript under preparation with co-authors from CSIC, UPM and UCA. PL2SP offers a non-destructive, statistically informed approach in the growth-characterization workflow that can complement TEM and AFM characterization and accelerate the optimization of nanostructures. This work on ensemble PL provides a robust foundation for future studies focused on single QD spectroscopy for more targeted investigations into the unique properties of individual QDs.

### Sb-soaked Quantum Dots for Enhanced Hole Spin manipulation

As mentioned above, the hole g-tensor can be manipulated with external voltages in type II InAs/GaAsSb QDs. ESR1 extended these results with theoretical calculations to prove that this approach is also viable for type I InAsSb QDs emitting in the O-band, with the added benefits of a type-I band alignment and the enhanced spin-orbit coupling (SOC) provided by the incorporated Sb. These nanostructures were grown at IMN-CSIC by applying an Sb-soaked step after QD formation [Taboada2010]. Sb exposure results in larger QDs, leading to a redshift in emission and a reduction in splitting to the first excited state. Sb segregation in the top half of the QDs draws the hole wavefunction from the flanks to the tip (Fig. W4.3.2b), reducing electron-hole overlap and mitigating strain-induced asymmetries, which explains the ~30% increase in radiative lifetime and the observed changes in MPL orbital splittings (Fig. W4.3.2d-g). Notably, magnetic field simulations using average size and composition values derived from PL2SP (in red) closely matched experimental results, outperforming simulations based on TEM measurements. Additionally, simulations indicate that electric fields applied to these tall Sb-graded QDs could double the g-factor swing compared to standard InAs QDs. These findings pave the way for designing SAQDs that are better optimized for spin-photon interface (SPI) applications.

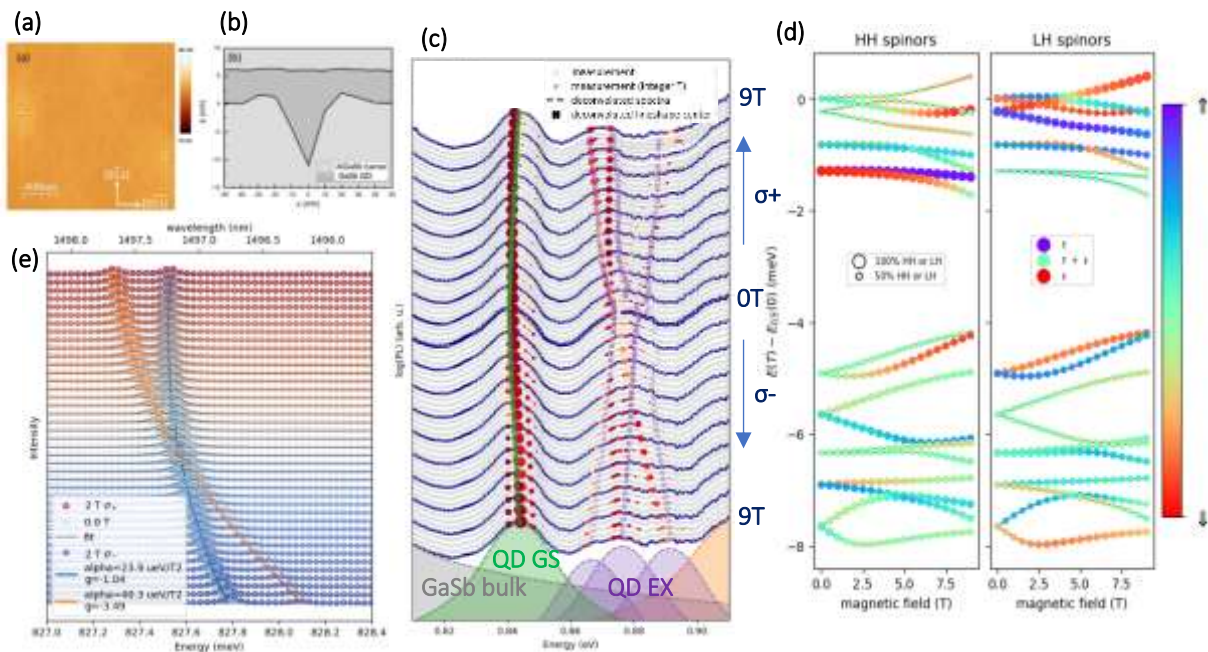
Further control at a single exciton level will be obtained once low-density Sb-soaked QD samples embedded in opportunely designed diode structure are provided. The samples available at IMN-CSIC and UPM did not have the low QD areal densities required for this, thus ESR1 and ESR3 (UPM) joined Wurzburg University (UWUE) for a 1 and 3-month secondments, respectively, aiming at their fabrication within a device of ESR1 design. The resulting samples are currently under investigation. This work on Sb-soaked QDs was first presented at the UK Semiconductors 2023 conference [Barbieri2023a], then further refined and presented at the first International Workshop on Quantum Antimonides Research & Upscaling (IQARUS2024) [Barbieri2024a], which took place the first three days of July 2024 in San Sebastián, Spain. A manuscript with the preliminary PL, TRPL and MPL ensemble characterization results is under preparation.



W4.3.2 TEM images from [Taboada2010] a) without and b) with Sb-exposure before capping. c) Electron (blue) and hole (red) ground state isosurfaces without and with 17% Sb in the top half. d)-g) MPL spectra on QD samples exposed to increasing Sb pressure before capping (left to right). Blue: deconvoluted experimental spectra, red: bright eh pairs from nextano simulations.

### Beyond Stranski-Krastanov growth mode for C-Band Emission

Adding Sb to Stranski-Krastanov (self-assembled) InAs QDs grown on GaAs substrates leads to a pronounced redshift of the emission, eventually arriving to the telecom C-band. However, this also brings changes in the confinement potential, type I to type II transition, and the QD size homogeneity as mentioned above. To solve this problem, the University of Tampere has proposed recently a new type of III-Sb nanostructures grown via nanohole filling with local droplet etching (LDE) directly on GaSb substrates, which emit close to the C-band [Chellu2021]. The system was initially simulated by ESR9 (TUB) [Leguay2024] and to explore the potential of this system as a spin-photon interface, ESR1 joined the Technical University of Berlin (TUB) for a two-month secondment so to extend the work and include external fields and a larger number of states (Fig. W4.3.3d). Besides QDs, the LDE growth mode inevitably leads to the formation of a lattice-matched quantum well (QW) of around 5/6 nm thickness in the samples. Equivalent strain-free quasi-2D GaAs/AlGaAs in magnetic fields have been studied extensively, but less is known on GaSb/AlGaSb QWs, which present stronger SOC and a  $\Gamma$ -L crossover around 4-5 nm of thickness. The MPL spectra from these nanostructures is therefore richer in phenomenology.



W4.3.3 a) AFM image of nanoholes on AlGaSb, indicate a QD density lower than 1 QD per  $\mu\text{m}$ . b) AFM profiles before and after filling indicate a large inverted cone shape for the QDs. c) 0-9 T MPL, deconvolved with symmetric Voigt lineshapes, 1 for the ground state and 3 for the excited state. The overlaid nextnano results, in red-yellow, match well the orbital splittings. Larger dots indicate brighter recombination, Deep red indicates pure circular right/left polarization, yellow a combination of both. d) nextnano simulation of the energy shift in a magnetic field of the first 18 hole states. The size of the spot of the left (right) column relate to the heavy hole (light hole) component of the state. Spinor state purity is expressed with color. e) Deconvoluted  $\mu\text{MPL}$  of a single GaSb/AlGaSb QD measured from 0 to 2 T.

Simulations indicate that the relatively large size and lack of strain in these QDs result in well-defined shell structures for electron states, each with a clear spinor composition. In contrast, hole states are energetically clustered, with up to ten Kramers-degenerate states within the first 10 meV (Fig. W4.3.3d), exhibiting strong heavy-hole–light-hole (HH-LH) mixing and coupling. Thus, most electron-hole pairs become optically active. We attribute the energy shifts and orbital splittings in MPL mainly to electrons, with the quasi-continuum of holes contributing to the inhomogeneous broadening. Comparison between measurement and simulation shows good agreement nonetheless, as shown in Fig W4.3.3c. For the reasons above, ensemble MPL cannot quantify properly the g-factor, for which we started measuring single QD  $\mu\text{MPL}$  (Fig W4.3.3e). This work has been presented with posters both at the 12<sup>th</sup> international conference on Quantum Dots in Munich (QD2024) [Barbieri2024b] and at IQARUS2024 [Barbieri2024c] and a manuscript is under preparation.

A different approach using DE was also investigated. Using periodic alternated deposition of In and As, **IMN-CSIC** successfully grew DE InAs QDs on InP substrates, resulting in emission near the C-band. Time-resolved photoluminescence (TRPL) and magneto-photoluminescence (MPL) revealed that approximately 10% of the studied QDs exhibited clear zero-dimensional exciton features, with spectrometer-limited homogeneous linewidths ( $\sim 29 \mu\text{eV}$ ), well-defined parabolic diamagnetic shifts and Zeeman splittings, and fine structure splitting around  $88 \mu\text{eV}$ . These results highlight the potential of these QDs as single-photon emitters, while also emphasizing the need for improved growth control to increase the yield of isolated quantum emitters. This work was presented at iNOW2023 [Barbieri2023b].

In summary, **ESR1** advanced the understanding and development of the electronic and magnetic properties of III-Sb nanostructures for quantum technologies. Secondments from **CSIC** to **NEXTNANO**, **TUB** and **UWUE** enabled cross-training in different methods and techniques. By leveraging innovative growth techniques, such as Sb-soaked steps, droplet epitaxy, and local droplet etching, the work demonstrated the potential of these materials for telecom C-band emission, spin-photon interfaces, and single-photon sources. The results highlight the importance of precise growth control and the integration of structural and optical feedback for optimizing QD properties. These efforts pave the way for future studies, particularly in single-QD magneto-optical spectroscopy, enabling further exploration of III-Sb materials for quantum communication applications. A spin-out of **CSIC**, G2ZERO SL, has shown interest on these results to shift the emission from NIR to telecom of their patent protected g2-Zero<sup>®</sup> single photon device technology.

#### References WP4.1

[Acar2024] G Acar, S Jones, P Hodgson, F. Alvarado-Cesar, R. Beanland and M Hayne (2024) "Novel GaSb Quantum Ring Light Emitting Diodes (QR-LED) with Distributed Bragg Transmitter (DBT) Operating at Telecommunication Wavelengths" SIOE conference, Cardiff, UK 2-4 April 2024

[Hodgson2022] P. D. Hodgson, D. Lane, P. J. Carrington, E. Delli, R. Beanland, and M. Hayne (2022) "ULTRARAM: A Low Energy, High Endurance, Compound-Semiconductor Memory on Silicon." *Advanced Electronic Materials* **8** 2101103 <https://doi.org/10.1002/aelm.202101103>

[Petrovic2024] B. Petrovic, A. Bader, J. Nauschuetz, T. Sato, S. Birner, R. Weih, F. Hartmann and S. Hoefling (2024) "5.0um emitting interband cascade lasers with superlattice and bulk AlGaAsSb claddings." *J Vacuum Science and Technology B* **42** 043202 <https://doi.org/10.1116/6.0003584>

[Trevisan2023] A. Trevisan, P. D. Hodgson, D. Lane, M. Hayne, and P.M. Koenraad, (2023) "Defect formation in InGaAs/AlSb/InAs memory devices" *J Vacuum Science and Technology B* **41** 0444001 <https://doi.org/10.1116/6.0002677>

#### References WP4.2

[Dolado2023a] J. Dolado et al. "Interplay between Crystal Structure and Optical Response in Plateau-Rayleigh Zn<sub>2</sub>GeO<sub>4</sub> /SnO<sub>2</sub> Heterostructures" *Adv. Photonics Res.* **4**, 2300063 <https://doi.org/10.1002/adpr.202300063>

#### References WP4.3

[Barbieri2022] Giulio Barbieri et al "Genetic-Algorithm-Based Simulation of Self-Assembled Quantum Dot Photoluminescence Spectra", IEEE NANO 2022, Palma de Mallorca, ES, Oral presentation.

[Barbieri2023a] Giulio Barbieri et al "Linking structural, optical, and magneto-optical properties of InAsSb/GaAs quantum dots through genetic optimization algorithms", UK Semiconductors 2023, Sheffield, UK, oral presentation.

[Barbieri2023b] Giulio Barbieri et al. "InAs/InP quantum dots grown by solid source MBE with emission at 1550 nm." (2023). iNOW 2023, Wurzberg, DE, poster.

[Barbieri2024a] Giulio Barbieri et al "Sb-soaked InGaAs/GaAs quantum dots for enhanced hole g-tensor modulation", IQARUS 2024, San Sebastian, ES, oral presentation.

[Barbieri2024b] Giulio Barbieri et al "Magneto-optical properties of droplet-etched strain-free GaSb/AlGaSb QDs emitting at 1.5  $\mu\text{m}$ ", QD2024, Munich, DE, poster.

- [Barbieri2024c] Giulio Barbieri et al "MagnetoOptoelectronic properties of local droplet etched GaSb/AlGaSb quantum dots emitting in the S-band", IQARUS 2024, San Sebastian, ES, poster.
- [Chellu2021] Chellu, Abhiroop, et al. "Highly uniform GaSb quantum dots with indirect–direct bandgap crossover at telecom range." *APL Materials* 9.5 (2021).
- [Fuster2009] Fuster, David, et al. "Direct formation of InAs quantum dots grown on InP (001) by solid-source molecular beam epitaxy." *Applied Physics Letters* 94.13 (2009).
- [Leguay2024] Leguay, Lucie, et al. "Unveiling the electronic structure of GaSb/AlGaSb quantum dots emitting in the third telecom window." *Materials for Quantum Technology* 4.1 (2024): 015401.
- [Llorens2019] Llorens, J. M., et al. "Topology driven g-factor tuning in type-II quantum dots." *Physical Review Applied* 11.4 (2019): 044011.
- [Taboada2010] Taboada, Alfonso G., et al. "Structural and optical changes induced by incorporation of antimony into InAs/GaAs (001) quantum dots." *Physical Review B—Condensed Matter and Materials Physics* 82.23 (2010): 235316.